Micromechanics-Based Predictive Model for Compressively Loaded Angle-Ply Composite Laminates

Jung Hyun Ahn,* and Anthony M. Waas[†]
University of Michigan, Ann Arbor, Michigan 48109-2140

A micromechanics-based analysis to predict damage initiation in compressively loaded symmetric angle-ply laminates is described. The finite element method in conjunction with the commercial code Abaqus is used to solve the governing system of equations. The results obtained for the predictions are compared against a set of experimental results previously made available for AS4/3502 symmetric angle-ply laminates. A unified model that captures damage initiation and that describes failure mode transition as a function of ply angle is reported. The prediction of the model is found to compare favorably against the experimental data.

I. Introduction

THE response of composite laminates when subjected to mechanical loads is influenced by the material type and stacking sequence adopted. In order to exploit the multitude of beneficial factors that composite laminates have to offer, it is important to gain a thorough understanding of how the response to mechanical loads and ultimate failure stress are related to the laminate microstructure. The compressive strength of laminates is an important design parameter for aerospace structures made of composite laminates. Indeed, the problem of predicting compressive strength has received considerable attention in the recent literature, as evidenced by the large number of research papers discussed in, for example, the survey papers by Waas and Schultheisz[1] and Schultheisz and Waas.[2] Previous experimental and analytical results pertaining to the static compressive strength of a laminate based on a unidirectional polymer matrix have established that fiber microbuckling in the presence of a nonlinear matrix is the dominant mode of compressive failure in these laminates. These results have been thoroughly discussed by Budiansky and Fleck,[3] Kyriakides et al.,[4] Sun and Jun,[5] and Schapery.[6,7] Similar investigations that account for time-dependent effects have been presented by Sun and Thiruppukuzhi,[8] Weeks and Sun,[9] Woldesenbet and Vinson,[10] Hsiao and Daniel,[11] Hsiao et al.,[12] Oguni and Ravichandran,[13] and Lee and Waas.[14] The importance of establishing the connection between the unidirectional compressive strength and the compressive strength of a laminate that has multidirectional plies (with zero plies included) has received lesser attention, although Drapier et al.,[15] Swanson,[16] Swain et al.,[17] Lesko et al.,[18] and Xu et al.,[19] have introduced models that capture some of the effects of stacking. The situation becomes less satisfactory when one examines the compressive strength of angle-ply laminates (no zero plies). Rotem and Hashin[20] and Kim[21] conducted experimental studies of angle-ply laminates and found that shear failure mechanisms were significant. Shuart[22] conducted a careful and systematic experimental study on the compression failure of $(+\theta/-\theta)_{ns}$ laminates made of AS4/3502 epoxy. Shuart was able to identify the transition of failure between fiber microbuckling/kink banding (which he also called fiber brooming, because sometimes the laminate broke along the band that was formed near the boundary of the loaded edge), in-plane matrix shearing, and matrix compression. No unifying model was introduced to capture the different regimes of failure. Instead, different simplified analytical models were constructed to explain the different failure mechanisms, which change as a function of ply angle. However, Shuart presented a complete set of experimental data to show the different mechanisms of failure as well as the dependence of laminate compressive strength on the ply angle.

In the present paper, we report the results from a micromechanics-based finite element analysis that was used to model the microstructural aspects of the response and failure of an angle-ply laminate subjected to compression loads. This analysis incorporates the nonlinear constitutive response of the matrix, which plays a crucial role in the failure mechanism. Shuart's experimental data for the laminate failure have been used here as a benchmark for the trends to be expected when the compressive failure of angle-ply laminates is investigated, as well as for comparison against the analysis predictions. Good agreement between the model predictions and the experimental results is found.

II. Mechanical Model for Compressive Response of an Angle-Ply Lamina

The configuration studied is as shown in Fig. 1, where an angle-ply laminate, $(\pm\theta)_{ns}$, is subjected to uniform compression loading. The (x, y) axes denote the lamina orthotropic axes, and the $(1, 2)$ axes denote the orthotropic material axes. The approach taken here mirrors the earlier work of the authors,[23] in which a microregion situated in an area of intense stress is modeled as an array of alternating layers of fiber and matrix. In the present context, there is no prefrntial location for the microregion, because each lamina is in a state of homogeneous deformation.

A microregion with dimension $H \times W$ is of interest for the finite element analysis. First, the compliances of a lamina in the x–y coordinate frame are related to the orthotropic compliances in the 1–2 coordinate frame by

$$S_{xx} = m^4 S_{11} + n^4 S_{22} + 2m^2 n^2 S_{12} + m^2 n^2 S_{66}$$

$$S_{yy} = n^4 S_{11} + m^4 S_{22} + 2m^2 n^2 S_{12} + m^2 n^2 S_{66}$$

$$S_{xy} = m^2 n^2 S_{11} + m^2 n^2 S_{22} + (m^4 + n^4) S_{12} - m^2 n^2 S_{66} \quad (1)$$

where $m = \cos(\theta)$ and $n = \sin(\theta)$. The orthotropic compliances S_{11}, S_{22}, and S_{66} are computed by using the lamina properties listed in Table 1, and the relations among lamina properties and compliances are as given in Hyer.[24] From Eq. (1) and with the use of classical lamination theory, the laminate engineering properties E_{xx}, E_{yy}, G_{xy}, and v_{xy} are computed. These values are shown in Table 2. When these values and a loading condition of unit compressive stress in the x direction are used, the laminate strains are found from

$$\begin{bmatrix} \epsilon_{xx} \\ \epsilon_{yy} \\ \gamma_{xy} \end{bmatrix} = \begin{bmatrix} 1/E_{xx} & -v_{xy}/E_{xx} & 0 \\ -v_{xy}/E_{xx} & 1/E_{yy} & 0 \\ 0 & 0 & 1/G_{xy} \end{bmatrix} \begin{bmatrix} \sigma_{xx} = -1 \\ \sigma_{yy} = 0 \\ \tau_{xy} = 0 \end{bmatrix} \quad (2)$$

Once the laminate strains in the x–y coordinate frame are obtained, it is necessary to transform the laminate strains to the 1–2

Table 1   Lamina properties of AS4/3502

E_{11}, Psi	E_{22}, Psi	G_{12}, Psi	ν_{12}
18.5×10^6	1.63×10^6	0.87×10^6	0.3

Table 2   Engineering properties of $(\pm 45)_{ns}$ AS4/3502[a]

E_{xx}, Psi	E_{yy}, Psi	G_{xy}, Psi	ν_{xy}
3.87×10^6	3.87×10^6	4.625×10^6	0.68

[a]These are the properties obtained by Shuart.[22]
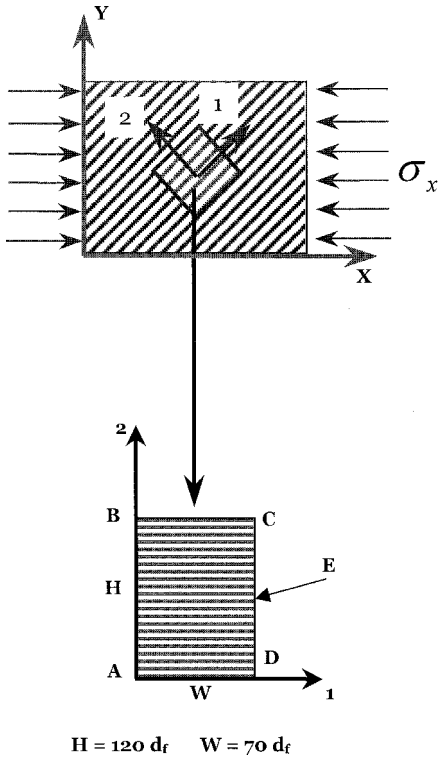

$$H = 120 \, d_f \qquad W = 70 \, d_f$$

Fig. 1   Problem configuration.

coordinate frame for the purpose of specifying displacement boundary loading in the ensuing finite element analysis. Thus,

$$\begin{bmatrix} \epsilon_{11} \\ \epsilon_{22} \\ \frac{1}{2}\gamma_{12} \end{bmatrix} = [T] \begin{bmatrix} \epsilon_{xx} \\ \epsilon_{yy} \\ \frac{1}{2}\gamma_{xy} \end{bmatrix} \qquad (3)$$

where $[T]$ is given by

$$[T] = \begin{bmatrix} m^2 & n^2 & 2mn \\ n^2 & m^2 & -2mn \\ -mn & mn & m^2 - n^2 \end{bmatrix} \qquad (4)$$

In the finite element analysis that follows, the microregion is fixed at the origin of the orthotropic material coordinate frame, because the displacements are measured with respect to this point. Then, the displacement fields corresponding to the strain state (3) are given by

$$u(x, y) = \epsilon_{11}[x - (W/2)] + \gamma_{12}/2[y - (H/2)]$$

$$v(x, y) = \epsilon_{22}[y - (H/2)] + \gamma_{12}/2[x - (W/2)] \qquad (5)$$

With the use of Eq. (5), the displacements corresponding to the node location of the boundaries of the microregion were computed. These values were then used as boundary loading in the finite element analysis that is described later.

III.   Characterization of the In Situ Matrix Property

In Shuart's paper,[22] along with the experimental results, the elastic properties of the lamina and the complete shear stress–shear strain behavior of a AS4/3502 in the orthotropic material coordinate system, obtained according to the procedure described in Daniel and Ishai,[25] is shown. This response curve is reproduced here as Fig. 2. The procedure used to generate the data consists of subjecting a $(\pm 45)_{ns}$ angle-ply laminate to uniaxial compression and measuring the laminate strains ϵ_{xx} and ϵ_{yy} and the applied remote stress on the laminate. Note that, for this test, $\gamma_{xy} = \epsilon_{xx} - \epsilon_{yy}$. The data in Fig. 2 can be used to extract the complete nonlinear shear stress–shear strain response of the in situ matrix (3502) as discussed as follows.

We begin by assuming that the 3502 matrix material can be modeled as an elastic-plastic solid obeying the small strain $J2$ flow theory of plasticity.[26] Then, from the elastic (linear) portion of the curve in Fig. 2, we first obtain the in-plane lamina shear modulus G_{12}. Furthermore, as shown in Daniel and Ishai,[25] for a balanced symmetric 45-deg angle-ply laminate, the major Poisson ratio ν_{xy} is given by

$$\nu_{xy} \cong \frac{E_{11} - 4G_{12}}{E_{11} + 4G_{12}} \qquad (6)$$

Thus, with Eq. (6), we can obtain the values of the two strain components, ϵ_{xx} and ϵ_{yy}, corresponding to each data point in Fig. 2. Here we are assuming that the in-plane Poisson ratio ν_{xy} given by Eq. (6) holds throughout the deformation history. In the lamina orthotropic coordinates, we know that

$$\epsilon_{11} = \epsilon_{22} = (\epsilon_{xx} + \epsilon_{yy})/2, \qquad \gamma_{12} = 2\epsilon_{12} = \epsilon_{xx} - \epsilon_{yy} \quad (7)$$

$$\sigma_{11} = -\sigma_{xx}/2, \qquad \sigma_{22} = -\sigma_{xx}/2, \qquad \tau_{12} = -\sigma_{xx}/2 \quad (8)$$

Thus, with the use of Eqs. (7) and (8) and the definitions of equivalent stress, $\bar{\sigma}$, and equivalent plastic strain increment, $\bar{d}\epsilon^p$ (defined in the Appendix), the data in Fig. 2 can be used to construct a plot of $\bar{\sigma}$ against $\bar{\epsilon}^p$ (Fig. 3).

According to the $J2$ flow theory of plasticity with a Mises–Henky yield condition, the ratio of the increment of each plastic strain component to its corresponding deviatoric stress component remains constant; that is,[26]

$$d\epsilon_{ij}^p / \hat{\sigma}_{ij} = d\lambda \qquad (9)$$

When Eq. (9) and the relation between $\bar{\sigma}$ and $\bar{d}\epsilon^p$ are used, the nonlinear portion of the shear stress (τ_{12})–shear strain (γ_{12}) response curve for a single lamina can be extracted. The curve thus obtained for AS4/3502 is shown in Fig. 4. The instantaneous slope of the curve in Fig. 4 is the tangent shear modulus of the lamina, $G_{12}(\tau_{12})$. Therefore we next use the Halpin–Tsai relations (Daniel and Ishai[25]), which follow, to extract the variation of the in situ matrix shear modulus $G_m(\tau_{12})$.
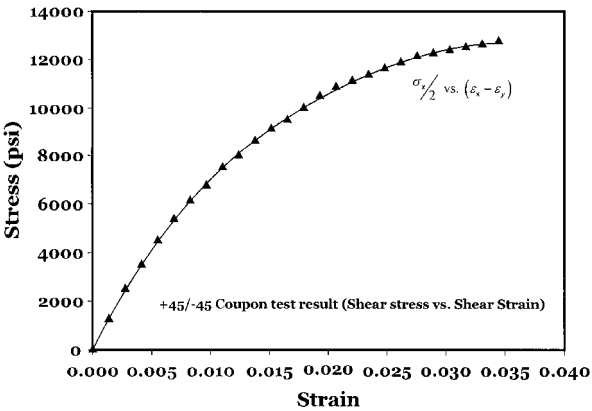

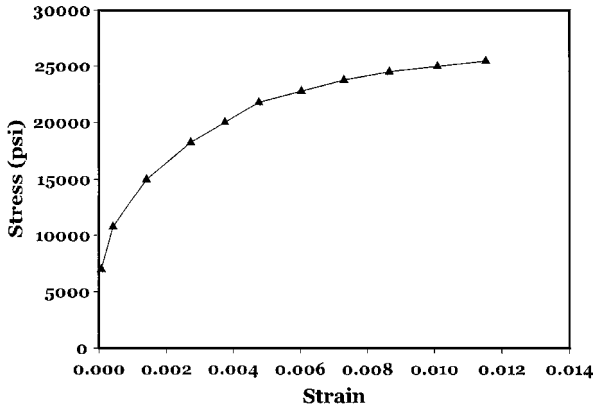**Fig. 2   Shear stress vs shear strain response of a AS4/3502 lamina as obtained by Shuart.[22]**

Fig. 3 Equivalent stress $\bar{\sigma}$ vs equivalent plastic strain $\bar{\epsilon}^p$ for AS4/3502, deduced from Fig. 2.
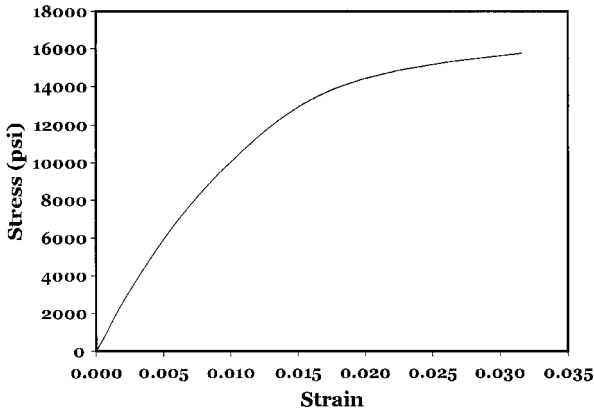

Fig. 4 Shear stress τ_{12} vs shear strain γ_{12} curve for AS4/3502 based on $J2$ flow theory of plasticity and the data in Fig. 2.
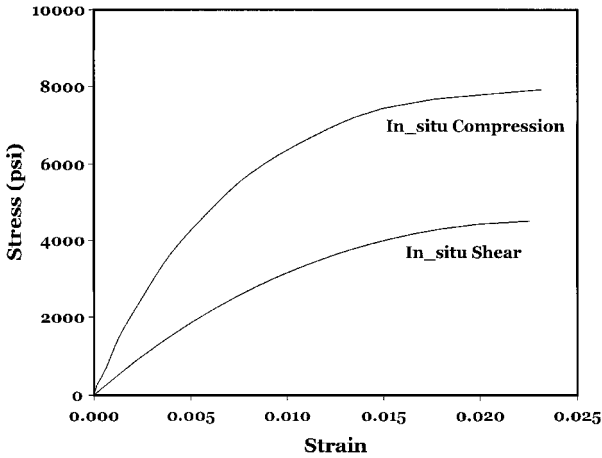

Fig. 5 In situ shear stress vs shear strain response of the matrix and the deduced uniaxial stress vs uniaxial strain response of the matrix.

$$G_{12} = G_m \frac{1 + \zeta_2 \eta_2 v_f}{1 - \eta_2 v_f}, \qquad \eta_2 = \frac{G_{12f} - G_m}{G_{12f} - \zeta_2 G_m} \qquad (10)$$

In addition, $\zeta_2 = 1$ for the random packing of fibers. With $G_m(\tau_{12})$ so obtained, the in situ matrix shear stress–shear strain curve is as shown in Fig. 5. In a similar manner, the in situ uniaxial stress–strain curve in compression for the matrix is also obtained. This uniaxial response curve is used in the input data file for the finite element analysis that follows. This curve is also shown in Fig. 5.

IV. Finite Element Analysis Modeling

The region to be analyzed using the finite element analysis (FEA) is as shown in Fig. 1, where a rectangular domain of dimension H ($120 \, d_f$, fiber diameter) $\times W$ ($70 \, d_f$) of alternate layers of fiber and matrix are considered in a plane-strain setting. The matrix layers have a thickness that provides the correct overall fiber volume fraction, $V_f = 55\%$, in the present case. The fiber is modeled as an elastic solid with the properties as indicated in Table 1, and the matrix is modeled as a elastic-plastic isotropic solid that undergoes finite deformation, obeying the $J2$ flow theory of plasticity with isotropic hardening. The in situ uniaxial stress–strain response of the matrix is as indicated in Fig. 5. The fiber and matrix layers are discretized with the CPS4 finite element by using the commercial code Abaqus. The total number of degrees of freedom for the baseline model is approximately 5754, which consists of 1498 fiber and 1242 matrix elements. In the mesh sensitivity study to be discussed later, the size of this baseline model is increased gradually to study its dependence on the predicted compressive load-carrying capability.

For the displacement data on the boundaries of the microregion to be computed, the far-field loading on the angle ply was assumed to be a uniform compression stress $\sigma_{xx} = -1$, $\sigma_{yy} = 0$, $\tau_{xy} = 0$. Then the displacements were calculated by using the procedure described earlier. In particular, the displacements fields u $(1, 2)$, v $(1, 2)$ on the boundary of the microregion were computed. First, a linear static analysis of the microregion when subjected to displacement loading on the boundary was performed. Nodal equilibrium reaction forces at the boundaries were computed from such an analysis. Next, with the use of the Riks method[27] option available in Abaqus,[27] a nonlinear response analysis of the microregion was conducted, using the boundary nodal forces that are equal and opposite to the model reaction forces computed by means of the linear static run. This nonlinear response analysis incorporates the in situ nonlinear uniaxial stress–uniaxial strain relation of the matrix indicated in Fig. 5. As loading proceeds, the boundaries of the microregion undergo large rotations. To use nodal force loading, the multipoint constraint (MPC) option provided in Abaqus was used on the boundaries AB and CD of the microregion. In effect, this option allows these boundaries to remain straight yet undergo the correct global rotation and deformation, while maintaining equilibrium with the applied boundary loads. During the loading, the boundaries BC and DA of the microregion must be left free to deform into any shape that is in conformity with equilibrium requirements. Thus, deformation localization into bands within the microregion is allowed to develop, yet overall force equilibrium is maintained in the far field. Because the MPC option was used and the microregion size influences the observed results, a scaling and mesh sensitivity study was also carried out by systematically increasing the overall size of the microregion and performing the analysis as explained before.
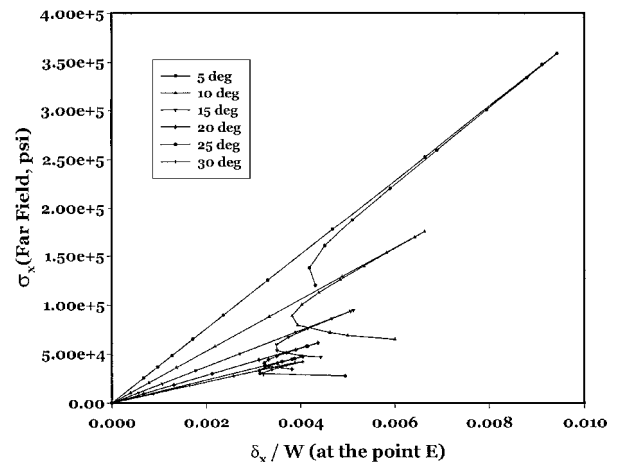

Fig. 6 Far-field stress (σ_x) vs normalized end shortening plots as a function of fiber angle ($5 \deg \le \theta \le 30 \deg$).
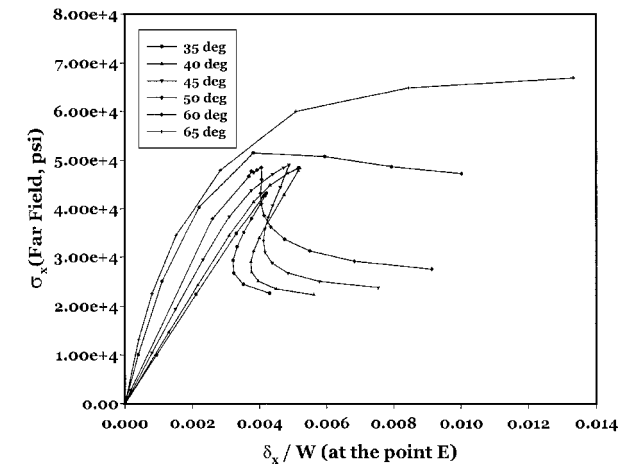
Fig. 7   Far-field stress (σ_x) vs normalized end shortening plots as a function of fiber angle (35 deg $\le \theta \le 65$ deg).
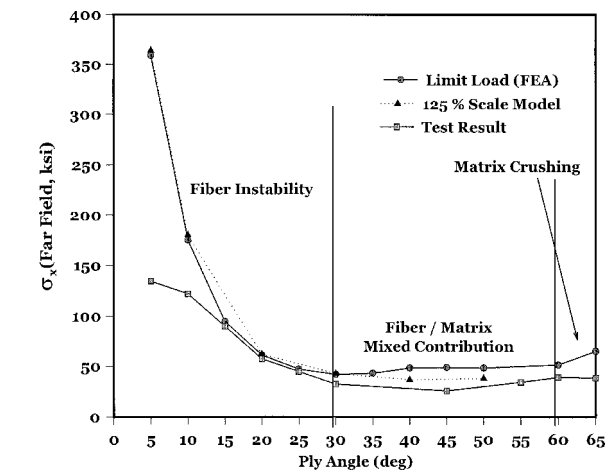

Fig. 8   Maximum stress as a function of ply angle: a comparison between prediction and experimental results reported by Shuart.[22]

V.   Finite Element Analysis Results and Interpretation

The finite element analysis results of the linear static run were verified by using the analytical solution of the corresponding linear elastic problem. Nonlinear load-response analyses were performed for 13 different configurations (5-deg to 65-deg ply-angle variation). A Riks analysis was performed as described, in which the solution was sought to a proportional loading case, including the possibility of unstable behavior. Typical response results are as shown in Figs. 6 and 7. In these figures, plots of the resultant axial stress, σ_x, in the far field as a function of normalized axial end shortening of the microregion (δ_x / W) for various ply angles are indicated (δ_x is evaluated at point E, indicated in Fig. 1). All of the curves show similar features, but with a different interpretation.

Initially, a typical response curve in Fig. 6 is linear, followed by an unstable unloading path from a maximum load for small ply angles (5 deg $< \theta <$ 30 deg), which eventually asymptotes to a constant value. This result can be explained in conjunction with experimental observations, in which a substantial drop in the axial load accompanies kink band formation at failure. This result also confirms various experimental results for unidirectional lamina (0-deg lamina), inferred from our result for $\theta = 5$ deg.

As the fiber angle increases, the dominant loading in the microregion is changed from fiber compression to shear deformation, where the matrix state of shear continuously increases in proportion. Now, the shear property of the matrix becomes dominant. Of course, the matrix layers are also subjected to axial compression and transverse compression, but it is the behavior in shear that is useful for interpreting the experimental results. As the ply angle increases, the initial slope of the response curve decreases for the ply-angle range (5–30 deg; Fig. 6), as expected. In addition, the maximum attainable load decreases and the unstable unloading path beyond the maximum load becomes a stable unloading beyond $\theta \cong 45$ deg (Fig. 7). That is, an abrupt load drop is no longer the case in an experimental setting. Instead, the slope beyond the load maximum indicates stable unloading and corresponding deformation localization into diffused broadbands. Further, beyond $\theta \cong 45$ deg, the dominant loading consists of matrix compression and shear, whereas the loads in the fiber direction (axial compression along the fibers) tend to decrease. Beyond $\theta \cong 60$ deg, a maximum load is no longer observed ($\theta = 65$ deg case; plotted in Fig. 7); instead, the microregion response indicates the gradual attainment of a stable plateau load. Response curves indicate a gradual "yield"-like behavior of the matrix. In these cases, one immediately sees that the fibers no longer provide additional stiffening to the matrix, because the predominant
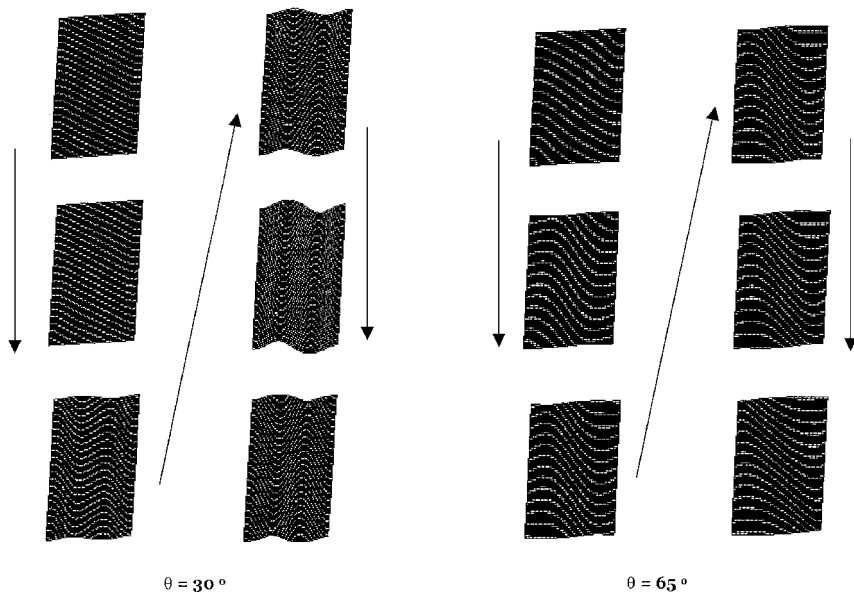

$\theta = 30°$

$\theta = 65°$

Fig. 9   Typical deformed shapes of microregion for $\theta = 35$ and 65 deg. Arrows indicate increasing order with respect to increasing amounts of load.
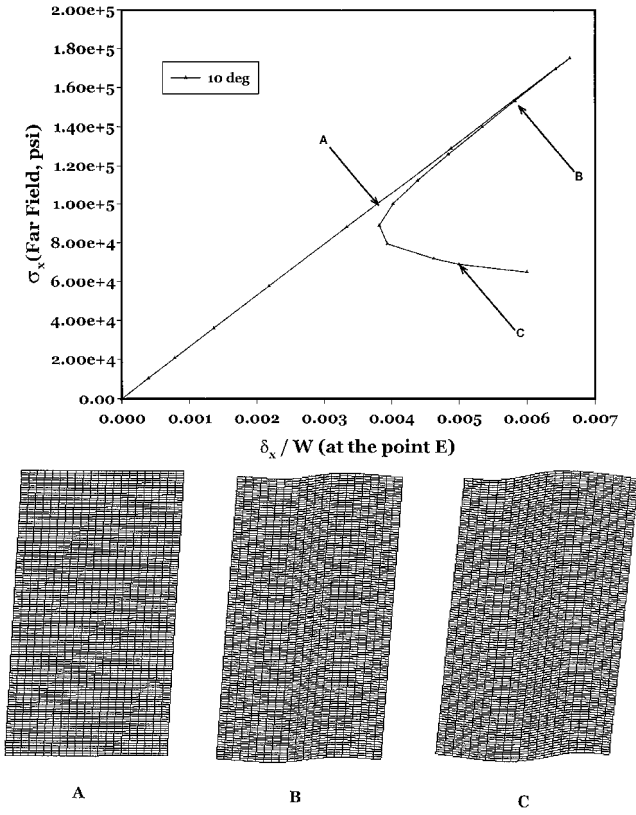
Fig. 10   Response curve for $\theta = 10$ **deg and deformed shapes of the microregion corresponding to points indicated in the response curve for** $\theta = 10$ **deg.**
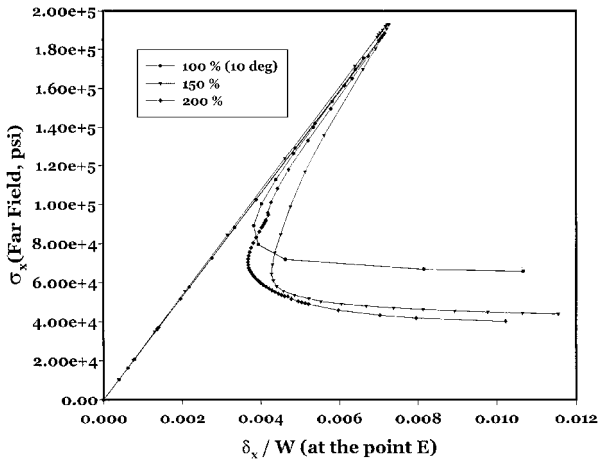

Fig. 11   Results of the mesh size sensitivity study ($\theta = 10$ **deg).**

loading occurs transverse to the fibers. Thus the matrix bears the brunt of the load. The plastic behavior of the matrix totally governs the deformation in these cases. A plot of the maximum (limit) load as a function of ply angle is shown in Fig. 8. Shuart's experimental data are also indicated for comparison. Another curve, corresponding to the limit load obtained with a larger mesh (all the dimensions of the microregion were increased by a factor of 1.25) is also indicated. The implications of these results for the maximum load and the results of a mesh sensitivity study are discussed next.

VI.   Discussion

As is evident from Fig. 8, the trends predicted by the present analysis based on the limit load, which corresponds to the onset (or initiation) of failure of the microregion, agree with the trends exhibited in the experimental results of Shuart. When the microregion is modeled and the in situ nonlinear matrix properties are incorporated, it is possible to follow the transition of the failure mode (unstable

failure initiation caused by fiber instability contrasted against matrix shear failure, indicated by a stable unloading path beyond the maximum load). Figure 9 indicates two series of deformed microregions corresponding to $\theta = 30$ and 65 deg, and Fig. 10 indicates the response of a microregion at a very low angle ($\theta = 5$ deg) where a steep load drop is observed. Notice that, for small angles, the bands of deformation localization are narrow, whereas as the angle increases, the deformation bands are diffused and broad. Just as observed by Shuart, the mechanism of compressive failure at low angles involves kink banding, leading to specimen splitting across the kinked band (accompanied by a large drop in load-carrying capacity); for larger angles (30 deg < θ < 50 deg), there is a transition in the failure mode where kinking does not occur. Instead, Shuart interpreted the failure as being fiber–matrix interfacial failure. At large angles (30 deg < θ < 50 deg), the interfacial shear stress is larger than that at the smaller angles. Furthermore, the matrix is predominantly loaded in shear with the attendant reduction in its shear stiffness. This scenario sets the stage for matrix plasticity to spread within the matrix layers, starting from the fiber–matrix interface. The fiber–matrix interfacial shear stress component in conjunction with any irregularities at the fiber–matrix interface (such as voids or partial debonding) leads to the onset of interfacial fiber–matrix failure. A complete analysis of the fiber–matrix interface fracture (which incorporates computing the energy release rates) necessitates a fracture-mechanics-based analysis with an accurate knowledge of the critical interfacial energy release rate measured by suitable experiments, as has been done, for example, in Song and Waas.[28] This aspect is not considered in the present analysis, but the reader is referred to Song and Waas[28] for further details. Instead, we have interpreted the experimentally observed fiber–matrix interfacial failure as being caused by the gradual weakening of the matrix integrity. Thus, the results in Fig. 8 for the maximum attainable stress of the microregion have a different interpretation as a function of θ. For (30 deg $\leq \theta \leq$ 65 deg), the maximum load is indicative of the onset of failure as a combined instability of the fiber and matrix.

In order to study mesh dependency of the predicted results, we present here the results of the 10-deg microregion study, because they are representative of what was observed for other angles. Three different microregion sizes were studied: the baseline microregion, and two scaled-up (all dimensions of the microregion increased by the same percentage) sizes of 150 and 200%. The results are as indicated in Fig. 11. Notice that the limit load is independent of the microregion size, whereas the plateau load appears to depend on the microregion size for this particular problem. This dependency can be easily understood by examining the physics of the failure mechanism. At the maximum load point, the fiber rotation in the soon-to-be-developed kink band is infinitesimal, but the matrix layers are loaded beyond their elastic limit. The unloading beyond the maximum load signals the period in which the localized deformation bands form and spread throughout the microregion. This stage is a transient stage; the attainment of a plateau load signifies the termination of the transient stage and the beginning of a steady-state process in which the localized band has developed across the microregion and undergoes further continued uniform deformation across the microregion. Thus, the transient stage alluded to herein is dependent on the size of the microregion (in particular, the transverse dimension, H, in Fig. 1); the larger the size, the lower the plateau load. What is important is the recognition that the limit load is independent of the size of the microregion and thus can be used with confidence as an indicator of the compressive strength of the laminate. The results we have presented here provide a unified picture associated with the prediction of compressive strength of angle-ply laminates.

VII.   Conclusions

Damage initiation in angle-ply laminated composites subjected to compressive loading has been investigated through a micromechanics-based finite element analysis. Comparison between experiment and the proposed analysis is good over a wide range of ply angles. Material properties of the fiber and matrix material that are readily available are used. In particular, matrix

nonlinearity is accounted for via $J2$ incremental plasticity theory. The present work is a nonempirical approach to predict compressive strength of angle-ply laminates.

Acknowledgments

Appendix: Definitions of Equivalent Stress and Plastic Strain

The equivalent stress and the equivalent plastic strain increment are defined as

$$\bar{\sigma} = \left\{ \frac{1}{2} \left[(\sigma_{11} - \sigma_{22})^2 + (\sigma_{22} - \sigma_{33})^2 + (\sigma_{33} - \sigma_{11})^2 \right] \right.$$
$$\left. + 3 \left[\tau_{12}^2 + \tau_{23}^2 + \tau_{31}^2 \right] \right\}^{\frac{1}{2}}$$

$$d\bar{\epsilon}_p = \left\{ \frac{2}{9} \left[\left(d\epsilon_{11}^2 - d\epsilon_{22}^p \right)^2 + \left(d\epsilon_{22}^p - d\epsilon_{33}^p \right)^2 + \left(d\epsilon_{33}^p - d\epsilon_{11}^p \right)^2 \right] \right.$$
$$\left. + \frac{4}{3} \left[d\epsilon_{12}^{p\,2} + d\epsilon_{23}^{p\,2} + d\epsilon_{31}^{p\,2} \right] \right\}^{\frac{1}{2}}$$

References

[1]Waas, A. M., and Schultheisz, C. R., *Compressive Failure of Composites, Part II, Progress in Aerospace Sciences*, Vol. 32, Elsevier, London, 1995, pp. 39–78.

[2]Schultheisz, C. R., and Waas, A. M., *Compressive Failure of Composites, Part I, Progress in Aerospace Sciences*, Vol. 32, Elsevier, London, 1995, pp. 1–39.

[3]Budiansky, B., and Fleck, N. A., "Compressive Failure of Fiber Composites," *Journal of Mechanics and Physics of Solids*, Vol. 41, 1993, pp. 183–211.

[4]Kyriakides, S., Arseculeratne, R., Perry, E. J., and Liechti, K. M., "On the Compressive Failure of Fiber Reinforced Composites," *International Journal of Solids and Structures*, Vol. 32, No. 6/7, 1995, pp. 689–738.

[5]Sun, C. T., and Jun, A. W., "Compressive Strength of Unidirectional Fiber Composites with Matrix Nonlinearity," *Composites Science and Technology*, Vol. 52, 1994, pp. 577–587.

[6]Schapery, R. A., "Compressive Strength Based on Local Buckling in Viscoelastic Composites," *Proceedings of Third Pan American Congress on Applied Mechanics*, Univ. of Iowa, Iowa City, IA, 1993.

[7]Schapery, R. A., "Prediction of Compressive Strength and Kink Bands in Composites using a Work Potential," *International Journal of Solids and Structures*, Vol. 32, No. 6/7, 1995, pp. 739–765.

[8]Sun, C. T., and Thiruppukuzhi, X., "Testing and Modeling of High Strain Rate Behavior of Polymeric Composites," *Composites Part B*, 1998, pp. 535–546.

[9]Weeks, C. A., and Sun, C. T., "Nonlinear Rate Dependent Response of Thick Section Composite Laminates," *High Strain Rate Effects on Polymer, Metal and Ceramic Matrix Composites and Other Advanced Materials*, edited by Y. D. S. Rajapakse and J. R. Vinson, Vol. 28, American Inst. of Mechanical Engineers, 1995, pp. 81–95.

[10]Woldesenbet, E., and Vinson, J. R., "Specimen Geometry Effects on High-Strain-Rate Testing of Graphite/Epoxy Composites," *AIAA Journal*, Vol. 37, No. 9, 1999, pp. 1102–1106.

[11]Hsiao, H. M., and Daniel, I. M., "Strain Rate Behavior of Composite Materials," *Composites Part B*, Vol. 29B, 1998, pp. 521–533.

[12]Hsiao, H. M., Daniel, I. M., and Cordes, R. D., "Strain Rate Effects on the Transverse Compressive and Shear Behavior of Unidirectional Composites," *Journal of Composite Materials*, Vol. 33, 1999, pp. 1620–1641.

[13]Oguni, K., and Ravichandran, G., "Dynamic Behavior of Fiber Reinforced Composites under Multiaxial Compression," *ASME Thick Composites for Load Bearing Structures*, AMD-Vol. 235, American Society of Mechanical Engineers, New York, 1999, pp. 87–96.

[14]Lee, S. H., and Waas, A. M., "Compressive Response and Failure of Fiber Reinforced Unidirectional Composites," *International Journal of Fracture*, Vol. 100, 1999, pp. 275–306.

[15]Drapier, S., Grandidier, J. C., and Potier-Ferry, M., "Theoretical Study of Structural Effects on the Compressive Failure of Laminate Composites," *C.R. Academcy of Science, Paris*, t.324, Series 2, 1997, pp. 219–227.

[16]Swanson, S. R., "A Micro-Mechanics Model for the In-Situ Compression Strength of Fiber Composite Laminates," *Journal of Engineering Materials and Technology*, Vol. 114, 1992, pp. 8–12.

[17]Swain, R. E., Elmore, J. S., Lesko, J. J., and Reifsnider, K. L., "The Role of Fiber, Matrix, and Interphase in the Compressive Static and Fatigue Behavior of Polymeric Matrix Composite Laminates," *Compression Response of Composite Structures*, Special Technical Publication 1185, American Society for Testing and Materials, Philadelphia, 1994, pp. 205–227.

[18]Lesko, J. J., Elmore, J. S., Case, S. W., Reifsnider, K. L., Dillard, D. A., and Swain, R. E., "A Global and Local Investigation of Compressive Strength to Determine the Influence of the Fiber/Matrix Interphase," *Compression Response of Composite Structures*, Special Technical Publication 1185, American Society for Testing and Materials, Philadelphia, 1994, pp. 228–240.

[19]Xu, Y. L., and Reifsnider, K. L., "Composite Compressive Strength Prediction Using a Nonhomogeneous Foundation Model," *Compression Response of Composite Structures*, Special Technical Publication 1185, American Society for Testing and Materials, Philadelphia, 1994, pp. 306–319.

[20]Rotem, A., and Hashin, Z., "Failure Modes for Angle Ply Laminates," *Journal of Composite Materials*, Vol. 9, 1975, pp. 191–206.

[21]Kim, R. Y., "On the Off-Axis and Angled-Ply Strength of Composites, Test Methods and Design Allowables for Fibrous Composites," ASTM STP 734, edited by C. C. Chamis, American Society for Testing and Materials, Philadelphia, 1989, pp. 91–108.

[22]Shuart, M. J., "Failure of Compression-Loaded Multidirectional Composite Laminates," *AIAA Journal*, Vol. 27, No. 9, 1988, pp. 1274–1279.

[23]Ahn, J. H., and Waas, A. M., "A Micromechanics Based Finite Element Model for Compressive Failure of Notched Uniply Composite Laminates Under Remote Biaxial Loads," *Journal of Engineering Materials and Technology*, Vol. 121, 1999, pp. 360–366.

[24]Hyer, M. W., *Stress Analysis of Fiber Reinforced Composite Materials*, WCB/McGraw–Hill, New York, 1997.

[25]Daniel, I. M., and Ishai, O., *Engneering Mechanics of Composite Laminates*, Oxford Univ. Press, New York, 1994.

[26]Lubliner, J., *Plasticity Theory*, Macmillan, New York, 1998.

[27]Abaqus, Ver. 5.8, Reference Manual, Vol. 1, Hibbit and Carlsson, 1998.

[28]Song, S. J., and Waas, A. M., "Energy-Based Mechanical Model for Mixed Mode Failure of Laminated Composites," *AIAA Journal*, Vol. 33, No. 4, 1995, pp. 739–745.